Polymer 51 (2010) 5807–5814

Contents lists available at ScienceDirect

Polymer

journal homepage: www.elsevier.com/locate/polymer

Nanolayer enhancement of biaxially oriented polypropylene film for increased gas barrier

Yijian Lin, Anne Hiltner*, Eric Baer

Department of Macromolecular Science and Engineering, Case Western Reserve University, Cleveland, OH 44106-7202, USA

ARTICLE INFO

Article history:
Received 27 August 2010
Received in revised form
24 September 2010
Accepted 28 September 2010
Available online 7 October 2010

Keywords:
Nanolayers
Biaxially orientated polypropylene
Oxygen permeability

ABSTRACT

An order of magnitude improvement in the oxygen barrier of biaxially oriented polypropylene (BOPP) films was achieved using a layer-multiplying, forced assembly process. The improvement was achieved without sacrificing clarity and toughness of the films. Sheets with 33 alternating layers of polypropylene (PP) (17 layers) and poly(ε-caprolactone) (PCL) (16 layers) were coextruded using layer-multiplication and two thick PP skins were added to the multilayered core as the last step in the continuous coextrusion process. The sheets were subsequently biaxially oriented to draw ratios from 4 × 4 to 6 × 6. Biaxial orientation at elevated temperature reduced the thickness of the melted PCL layers from the microscale to the nanoscale, which created 2-dimensional confinement for subsequent crystallization of the PCL layers. It was anticipated that the PCL layers would recrystallize as highly oriented, in-plane lamellae that would resemble single crystals. However, the PCL lamellae were oriented perpendicular to the film surface, which actually facilitated oxygen permeation through the PCL layers and increased the oxygen permeability of the oriented films. Crystallization as on-edge lamellae was attributed to nucleation by the polypropylene surface. However, the surface nucleation was prevented by inserting buffer polystyrene (PS) layers in between the PCL and PP layers. In this case, the PCL lamellae were oriented in-plane. With the very high aspect ratio lamellar crystals oriented perpendicular to the flux direction, the permeation pathway of oxygen became very tortuous and the oxygen barrier was significantly improved.

1. Introduction

Layer-multiplying coextrusion or “forced assembly” makes it possible to fabricate films that incorporate tens to thousands of polymer nanolayers. Previous studies using poly(ethylene oxide) (PEO) demonstrate a very dramatic decrease in gas permeability that can be achieved by confined crystallization of the nanolayers in such assemblies [1]. As the thickness of coextruded layers decreases from the microscale to the nanoscale, the morphology of PEO changes from 3-dimensional (3D) spherulites to 2-dimensional (2D) discoids and finally in 25 nm layers to in-plane lamellae that resemble large single crystals [2]. This crystallization habit imparts more than 2 orders of magnitude reduction in oxygen permeability to the PEO layers. The coextrusion process, which operates with readily available polymers, makes it possible to fabricate nanolayered polymeric structures in sufficient quantity to probe the structure–property processing relationships. For design and execution of packaging strategies, polymer nanolayers can be incorporated into conventional polymeric films to obtain the right barrier properties.

Commercial polymeric film processes often require an orientation step. For example, biaxially oriented polypropylene (BOPP) is a successful commercial product that is widely used for flexible food packaging. The biaxial drawing process transforms the brittle and opaque spherulitic morphology into a tough and transparent fibrous structure [3]. Good oxygen barrier is one of the key requirements, as well as clarity and toughness. Previous studies show that the oxygen permeability of BOPP film depends on the mobility of the amorphous tie-chains as measured by the β-relaxation intensity in dynamic mechanical thermal analysis experiments [4]. However, regardless of how the polypropylene is stretched, the achievable decrease in oxygen barrier is only about a factor of 2 compared to the unoriented polypropylene.

Various strategies have been attempted to improve the oxygen barrier of BOPP further, such as blending with impermeable fillers that have a large aspect ratio [5–8]. A large aspect ratio and a high degree of orientation create a tortuous pathway for gas transport, thereby reducing the permeability. Unfortunately, clarity of the film is sacrificed. The loss in light transmission is primarily due to light scattering at the interface between filler and matrix of differing

* Corresponding author.
E-mail address: ahiltner@case.edu (A. Hiltner).

0032-3861/$ – see front matter © 2010 Elsevier Ltd. All rights reserved.
doi:10.1016/j.polymer.2010.09.070

refractive index. In order to retain good clarity, it is necessary to reduce the thickness of the filler particle below the quarter wavelength of visible light. Exfoliated organosilicate platelets with thickness of a few nanometers and lateral dimension of hundreds of nanometers have the potential to enhance gas barrier while maintaining high transparency. Although considerable success was obtained with nylon 6 nanocomposites [9,10], a practical method for achieving good dispersion of exfoliated platelets in high volume polyolefins has proven an elusive goal [11].

Polymer single crystals with thickness of 20–30 nm and lateral dimensions of microns are another category of high aspect ratio, impermeable platelet-like nanoparticles. Coextruding nanolayers of a suitable crystallizable polymer such as PEO in a layered BOPP structure would produce impermeable single crystal-like lamellae appropriately oriented perpendicular to the direction of gas flux. However, the crystallizable nanolayers would be destroyed by the orientation process. Recently, we suggested an alternative approach for incorporating lamellar single crystals into BOPP film by *in situ* generation of the nanolayers [12]. An assembly with alternating layers of polypropylene (PP) and PEO is coextruded and subsequently biaxially stretched. The melted PEO microlayers are of an appropriate thickness so that stretching reduces them to nanolayers. During cooling, the nanolayers recrystallize as oriented lamellar single crystals of very high aspect ratio. Sensitivity to moisture is a major concern with PEO and indeed it is found that the permeability of PEO nanolayers increases by a factor of 2 at 85% relative humidity (RH) [12]. An alternative to PEO is needed. Here we investigate whether the phenomenon observed with PEO extends to other polymers, and in particular whether poly (ε-caprolactone) (PCL), which is considerably less sensitive to moisture than PEO, will also crystallize as nanolayers of in-plane lamellae that can be incorporated into BOPP films to reduce the gas permeability. Lastly, the clarity and mechanical properties of the BOPP films are tested.

2. Experimental

The PP (Polybond 3002, grafted with 0.2 wt% maleic anhydride) with melt flow index (MFI) of 7 g/10 min (2.16 Kg, 230 °C) was obtained from Chemtura Corporation. The PCL (Capa 6800) with molecular weight of 80,000 and MFI of 3 g/10 min (2.16 Kg, 160 °C) was obtained from Perstorp. The polystyrene (PS) (Styron 615) with MFI of 14 g/10 min (5 kg, 200 °C) was obtained from the Dow Chemical Company.

Sheets with 33 alternating layers of PP (17 layers) and PCL (16 layers) were coextruded using the layer-multiplying technique. Two thick PP skins were added to the multilayered core as the last step before the melt entered the sheet die. The total sheet thickness was about 380 μm. The core and the two skins were each about 125 μm thick. The total PCL in the sheets was 3.3%, 6.7%, and 10% by volume.

In order to prevent nucleation of PCL by the PP surface, 33 PS buffer layers were inserted between each of the PP layers and PCL layers. In the PP/PS/PCL sheets, the total PP/PS ratio in the skin and core combined was maintained at 85/15 in order to facilitate calculation of the PCL contribution to permeability. The total PCL content was 5, 10, and 15% by volume. In addition, a PP/PS control film with composition 85/15 was coextruded. The nominal layer thickness was calculated from the film thickness, the number of layers and the composition.

The coextruded multilayered sheets were biaxially oriented with a Brückner Karo IV biaxial stretcher. The best stretching temperature was found to be 150 °C for the PP/PCL sheets and 155 °C for the PP/PS/PCL sheets. The sheets were preheated at the stretching temperature for 60 s before they were simultaneously stretched in the two orthogonal directions. The stretching rate was 400% s^{-1} and draw ratios were 4 × 4, 5 × 5 and 6 × 6. Films that were directly cooled in air from the stretching oven were identified as air-quenched. The Brückner biaxial stretcher is equipped with a second oven that allows for thermal treatment of the stretched film before it is cooled and released from the grips. The second oven was used to isothermally crystallize films stretched to a draw ratio of 4 × 4. The stretched films are identified as nano-BOPP/PCL and nano-BOPP/PS/PCL.

A Perkin–Elmer Series 7 differential scanning calorimeter (DSC) was employed to record the first heating thermogram of coextruded multilayered sheets at a heating rate of 10 °C min^{-1} from 30 to 190 °C. In order to obtain the crystallization temperature of PCL nanolayers, the oriented films were first heated to 80 °C and held for 3 min. The cooling thermogram was then recorded at a cooling rate of 10 °C min^{-1}.

To view the layer morphology, a small specimen was cut from the coextruded sheet or the oriented film and microtomed at −85 °C through the thickness direction. The microtomed surface was examined in a Digital Laboratories Nanoscope IIIa atomic force microscope (AFM) operating in the tapping mode.

The O_2 permeability $P(O_2)$ of the oriented films was measured with a MOCON OX-TRAN 2/20 at 23 °C, 1 atm and 0% (or 85%) RH. Two films prepared under the same conditions were tested to obtain the average permeability. The CO_2 permeability $P(CO_2)$ was measured with a MOCON PERM-TRAN C4/40 at the same conditions. The CO_2/O_2 selectivity was calculated as the ratio of $P(CO_2)/P(O_2)$.

Wide angle X-ray scattering (WAXS) measurements were carried out using a rotating anode X-ray generator (Rigaku RU 300, 12 kW) equipped with two laterally graded multilayer optics in a side-by-side arrangement, giving a highly focused parallel beam of monochromatic CuK_α radiation ($\lambda = 0.154$ nm). Several thin films were stacked to get strong signals.

The clarity of the biaxially oriented films was quantified by light transmission measurements using an ultraviolet–visible spectrometer (Ocean Optics) [13]. To remove the surface scattering, mineral oil with refractive index of 1.500 was spread on both surfaces of the films. The diameters of the light source beam and the detector were both approximately 3 mm. The distance between film and detector was 6 mm. Five different spots on each film were selected to perform this measurement.

Toughness of the oriented films was tested in terms of the tear resistance and the puncture strength. The trouser tear test was carried out at ambient temperature according to ASTM D1938. An Instron 1122 tensile testing machine equipped with a 500 g load cell was employed to record the tear force at a speed of 250 mm min^{-1}. The puncture test was carried out with an MTS Alliance RT/30 tensile machine. Oriented films were loaded in a clamping device with a 10 mm diameter central hole. A sharp needle with 50 μm diameter tip was used to pierce the film at a rate of 30 mm min^{-1}.

3. Results and discussion

3.1. BOPP films with PCL nanolayers (nano-BOPP/PCL)

Coextruded sheets of PP/PCL microlayers were biaxially oriented at 150 °C [14], which was in the onset region of the PP melting endotherm and was higher than the melting temperature of PCL ($T_{m,PCL}$ = 57 °C), Fig. 1. During stretching, the melted PCL layers were squeezed by the adjacent PP layers and flowed in the two stretching directions, transforming the PCL from microlayers to nanolayers. Stretching to a 5 × 5 draw ratio reduced the thickness by 25×, which reduced the nominal PCL layer thickness, for example from 1.6 μm to 63 nm for BOPP/PCL-10%. Subsequent

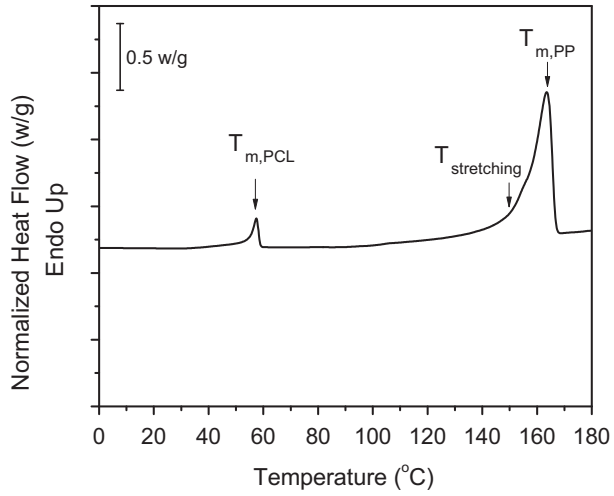

Fig. 1. First heating DSC thermogram of unstretched, coextruded PP/PCL-10% indicating the temperature at which the film was subsequently stretched ($T_{stretching}$).

cooling to ambient temperature allowed the PCL melt to crystallize within a 2D confined space. The stretched film is identified as nano-BOPP/PCL.

An AFM phase image shows the 16 continuous PCL layers in the layered core of a nano-BOPP/PCL film with 10% PCL, Fig. 2. The average PCL layer thickness was 70 nm which agreed well with the nominal layer thickness 63 nm. Because crystallization of PCL was confined in the nanolayers, growth of 3D spherulites was frustrated. It was anticipated from previous studies that the PCL would crystallize as highly oriented, in-plane lamella with large aspect ratio [1,2,12]. Such a structure would greatly increase the tortuosity of the diffusion pathway and thereby dramatically reduce the gas permeability. Oxygen permeability of the nano-BOPP/PCL films is given in Table 1. Unexpectedly, the oxygen permeability of the nano-BOPP/PCL films was slightly higher than that of the BOPP control film that was stretched under the same conditions.

Assuming that the permeability of the BOPP layers in nano-BOPP/PCL to be the same as in the control BOPP film, the effective oxygen permeability of the PCL nanolayers $P_{eff,PCL}$ was calculated according to the series model

$$P_{eff,PCL} = \frac{V_{PCL}}{\frac{1}{P_{film}} - \frac{V_{BOPP}}{P_{BOPP}}} \quad (1)$$

where V_{PCL} and V_{BOPP} are the volume fractions of PCL and PP, and P_{film} and P_{BOPP} are the oxygen permeabilities of the nano-BOPP/PCL film and the BOPP control film. The estimated permeability of the PCL layer barrer was substantially higher than that of the PCL control, e.g. $P_{eff,PCL} = 2.16$ barrer for nano-BOPP/PCL-7% and $P_{eff,PCL} = 46.2$ barrer for nano-BOPP/PCL-10%.

A 2D-WAXS pattern of the 5 × 5 stretched BOPP control showed four scattering rings at $2\theta = 14.1°$, 16.9°, 18.6°, 21.8° corresponding to the (110), (040), (130), and (111)/(041) planes of the α-form PP crystals. The concentration of intensity at specific angles revealed the high orientation of PP in the biaxially stretched film, Fig. 3a. In the 5 × 5 stretched nano-BOPP/PCL-10% film, additional scatterings from the PCL crystals were superimposed on the BOPP WAXS pattern, Fig. 3b. The meridional (200) scattering arcs ($2\theta = 23.4°$) of PCL indicated that the c-axis of the unit cell was oriented parallel to the layer plane. Therefore, the lamellae were oriented on-edge with the lamellar surfaces perpendicular to the plane of the film. The sharpness of the arcs indicated that the degree of orientation was

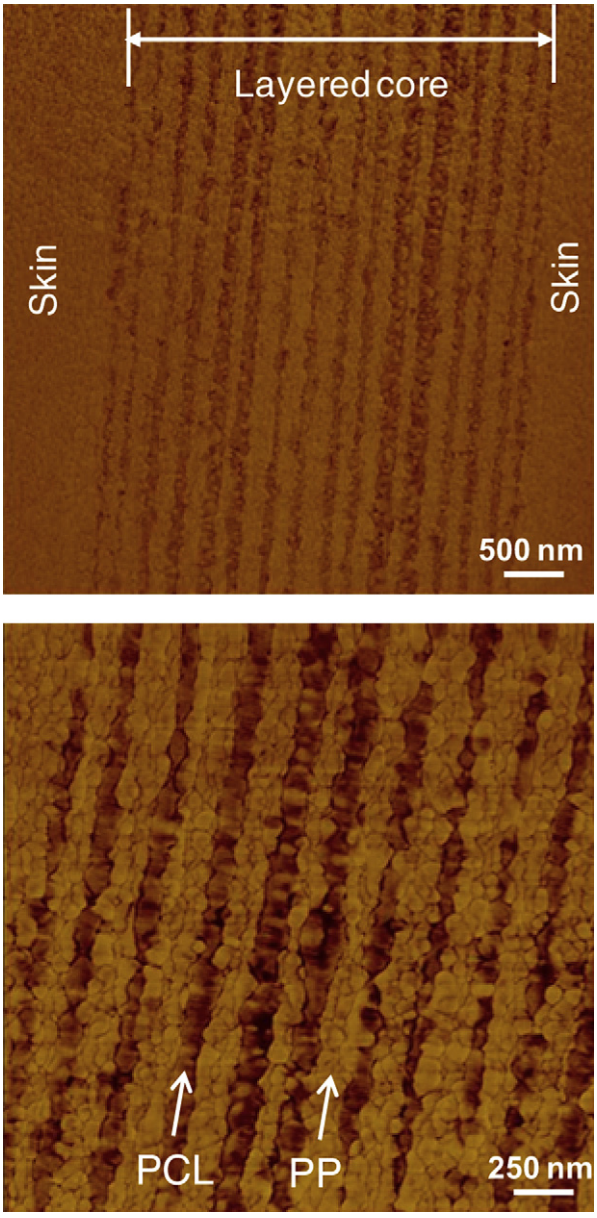

Fig. 2. The nanolayer morphology of the nano-BOPP/PCL-10% core after the film was stretched 5 × 5.

very high. The on-edge orientation should give 4-arc (110) scattering ($2\theta = 21.2°$), however these overlapped with the (130) scattering of PP. In order to obtain the scattering pattern of PCL only, the pattern of the BOPP control was subtracted from that of the nano-BOPP/PCL. The result shown in Fig. 3c revealed 4 (110) arcs at about 41°, 139°, 221°, and 319° in addition to the meridional (200) reflections. The on-edge oriented lamellae did not reduce the

Table 1
Oxygen permeability of nano-BOPP/PCL films.

Sample ($\lambda = 5 \times 5$)	Nominal PCL layer thickness l (nm)	P(O_2) of film P_{film} (barrer)
PCL control	–	0.983 ± 0.019
PP control	–	1.020 ± 0.021
BOPP control	–	0.635 ± 0.018
Nano-BOPP/PCL-3%	22	0.667 ± 0.016
Nano-BOPP/PCL-7%	43	0.666 ± 0.022
Nano-BOPP/PCL-10%	63	0.705 ± 0.020

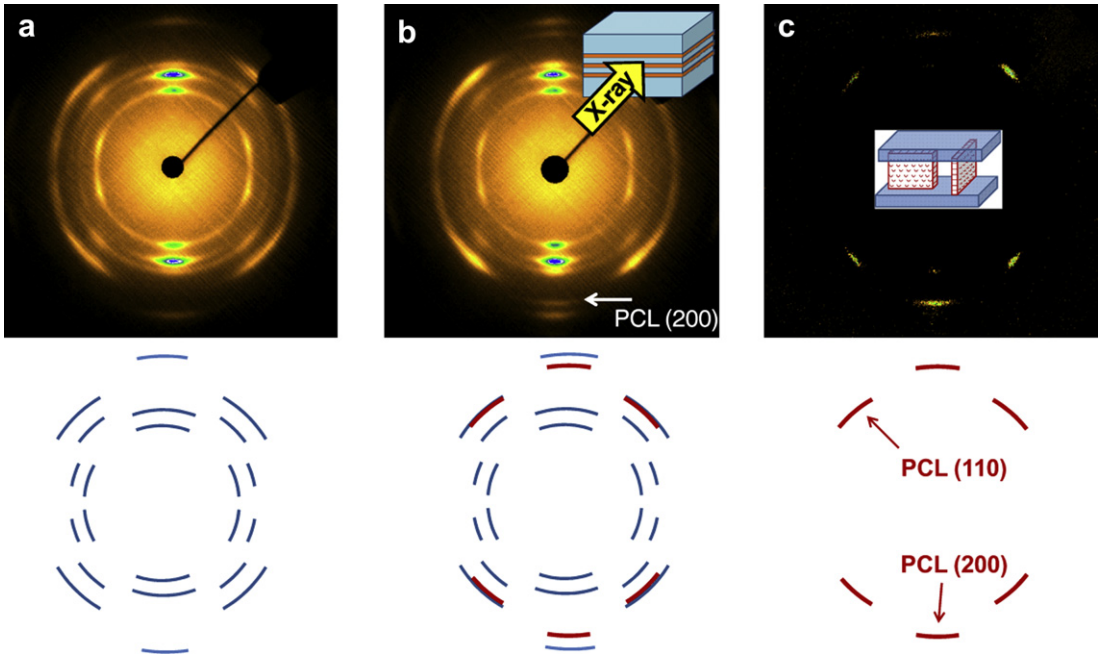

Fig. 3. 2D-WAXS patterns of (a) BOPP control film, (b) nano-BOPP/PCL-10% film, and (c) the PCL pattern obtained by subtracting (a) from (b). The draw ratio was 5 × 5.

permeability; on the contrary, the amorphous regions created permeable channels parallel to the flux direction which facilitated diffusion of the oxygen molecules.

The formation of on-edge PCL lamellae was attributed to nucleation of PCL crystals by the PP surfaces. Nucleation of PCL on polyolefins has been demonstrated previously. A polyethylene surface was shown to nucleate PCL [15,16], and PP was found to nucleate crystallization of PCL in melt blends [17]. This appears to be a surface phenomenon rather than epitaxial crystallization which involves specific lattice matching. The nucleating effect of PP was confirmed by comparing the crystallization temperature of PCL in nanolayers with that of a PCL control. The thermogram in Fig. 4 shows that the PCL control film (400 μm) crystallized at 30 °C with a crystallinity X_c of 38%. In contrast, the PCL in nano-BOPP/PCL crystallized 6 °C higher with a crystallinity of 41%.

3.2. BOPP/PCL films with PS buffer layer (nano-BOPP/PS/PCL)

It was necessary to prevent the surface nucleation of on-edge lamellae if enhanced barrier was to be achieved with large in-plane PCL lamellae. In order to provide an alternative interface for crystallization of the PCL, the layered core was coextruded with a thin buffer layer of amorphous polystyrene in between each of the PP and PCL layers. When the coextruded PP/PS/PCL sheets were biaxially oriented at 155 °C, the PS buffer layers were above the glass transition temperature (T_g = 101 °C) and were able to flow during biaxial stretching. The AFM phase image of a nano-BOPP/PS/PCL film that was stretched to 4 × 4 shows the PP and PCL layers separated by the continuous PS layers, Fig. 5. The nominal PCL layer thickness is 145 nm, PS layer thickness is 73 nm, and BOPP layer thickness is 245 nm.

The WAXS patterns of nano-BOPP/PS/PCL and the BOPP/PS control are compared in Fig. 6. In order to obtain the scattering pattern of PCL only, the pattern of the BOPP/PS control was subtracted from that of the nano-BOPP/PS/PCL. For the film that was stretched to 4 × 4, the (200) scattering arcs at 2θ = 23.4° and the (110) scattering arcs at 2θ = 21.2° were only observed on the equator. This was in contrast to the nano-BOPP/PCL where the reflections from the (200) planes were observed only on the meridian. The equatorial position of the (200) reflections indicated that the c-axis of the PCL unit cell was oriented perpendicular to the layer plane and therefore the lamellae were oriented in-plane. As the draw ratio increased, scattering features of the on-edge lamellar orientation began to appear. For the film with draw ratio of 6 × 6, the (200) scattering arcs were clearly seen in both the meridional and equatorial directions, Fig. 6c. The (110) equatorial scattering from the in-plane lamellae and the four (110) arcs from the on-edge lamellae were also observed. The latter were very weak and are almost invisible in the image. The mixture of in-plane and on-edge lamellae in films with the highest draw ratio was probably due to breakup of the PS layers. In places where the PS layer was broken, the PCL contacted the underlying PP layer, which nucleated on-edge crystallization.

The mixture of the two orientations was confirmed by the DSC cooling thermograms, Fig. 7. For the film that was stretched to

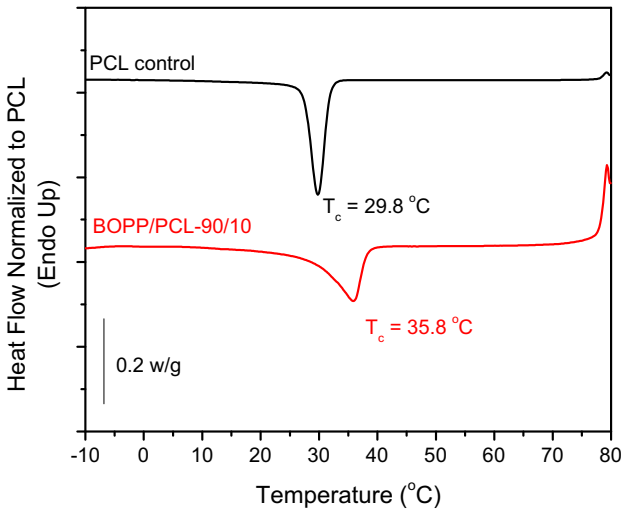

Fig. 4. DSC cooling thermograms of PCL control and BOPP/PCL-10% (draw ratio 5 × 5).

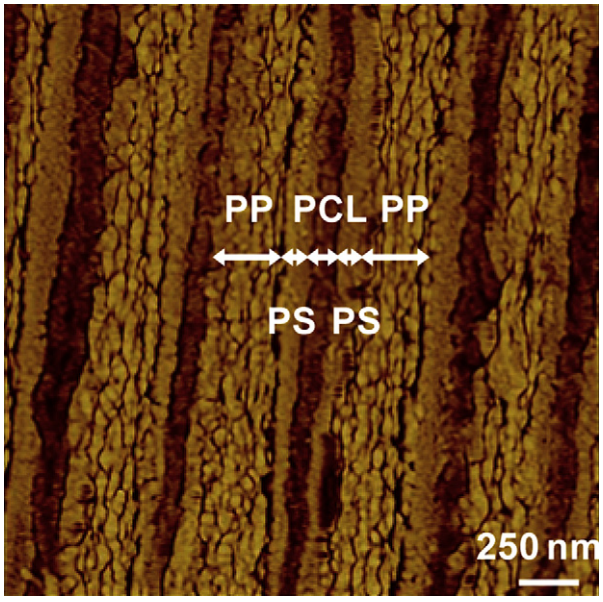

Fig. 5. Layer structure in the core of nano-BOPP/PS/PCL-15% film (draw ratio 4 × 4).

4 × 4, the crystallization exotherm occurred at a peak temperature of 26 °C with crystallinity X_c = 33%. As the draw ratio increased, a small shoulder appeared at 34 °C for the 5 × 5 film (X_c = 32%); the shoulder became more pronounced for the 6 × 6 film (X_c = 31%). The shoulder, which was close to the melting temperature of PCL in nano-BOPP/PCL, was attributed to the nucleation of PCL by the PP surface in places where the PS layers had broken up. The amount of exposed PP increased with the draw ratio.

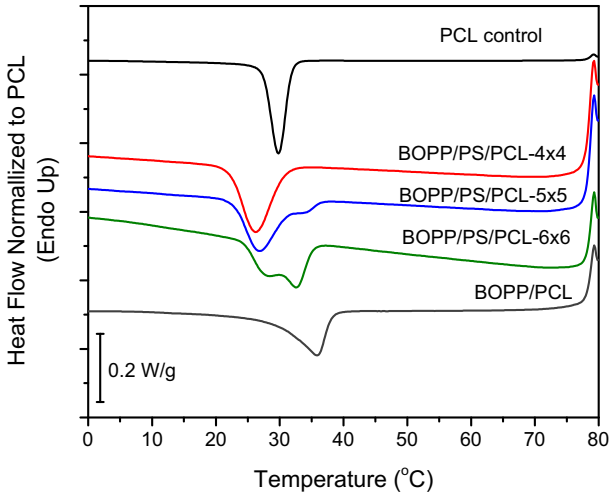

Fig. 7. DSC cooling thermograms of nano-BOPP/PS/PCL-10% with different draw ratios.

The BOPP/PS control had higher permeability than BOPP due to the higher permeability of PS (P_{PS} = 2.1 barrer), Table 2. However, the nano-BOPP/PS/PCL films had substantially lower oxygen permeability than the nano-BOPP/PCL films and the BOPP/PS control film, suggesting that the PS buffer layers indeed produced in-plane orientation of the PCL lamellae rather than the on-edge orientation found with nano-BOPP/PCL. With the lamellae oriented perpendicular to the flux direction, they effectively increased the tortuosity of diffusion pathway and enhanced the gas barrier. The effective oxygen permeability of the PCL layer in the nano-BOPP/PS/PCL films was calculated according to

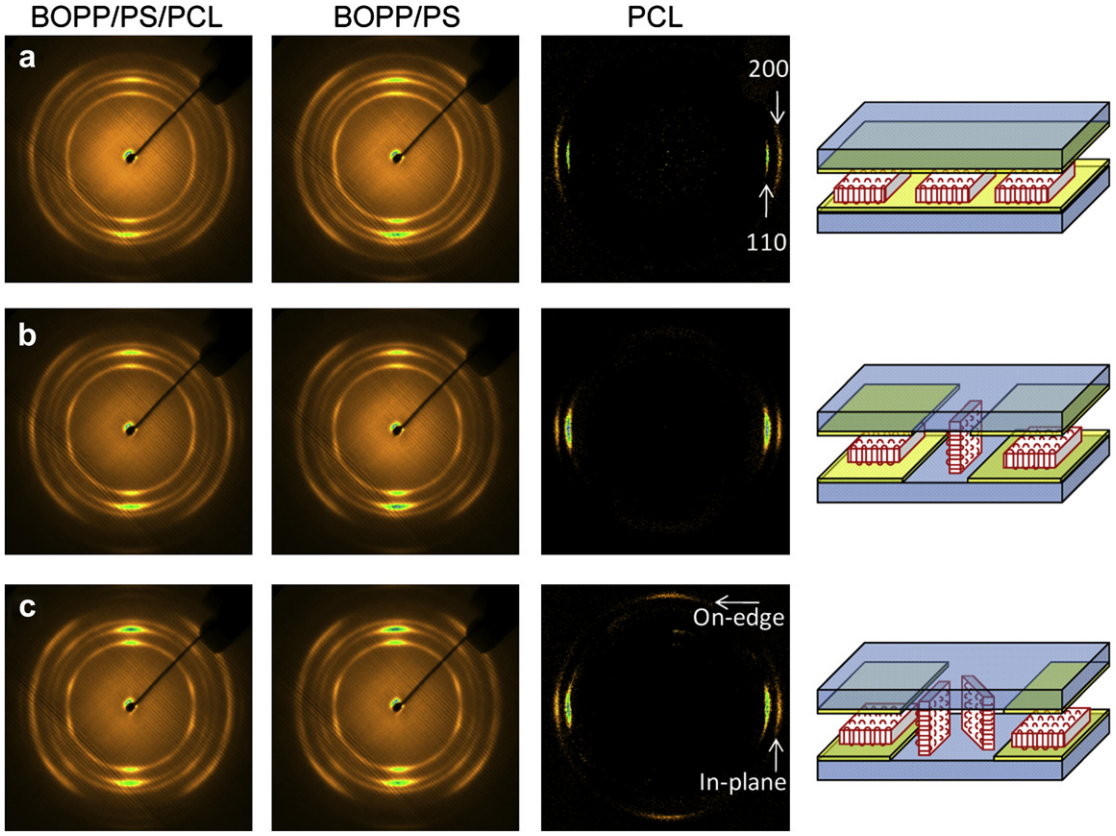

Fig. 6. 2D-WAXS patterns of BOPP/PS/PCL-10% films that were stretched to (a) 4 × 4 (b) 5 × 5 and (c) 6 × 6. The PCL patterns were obtained by subtraction.

Table 2
Oxygen permeability of nano-BOPP/PS/PCL films.

Sample	Nominal PCL layer thickness l (nm)	P(O_2) of film P_{film} (barrer)	Effective P(O_2) of PCL layer $P_{eff,PCL}$ (barrer)	Aspect ratio of lamellae α
BOPP/PS-4 × 4	–	0.777 ± 0.002	–	–
BOPP/PS/PCL-5%-4 × 4	45	0.468 ± 0.003	0.0547	101
BOPP/PS/PCL-10%-4 × 4	94	0.442 ± 0.033	0.0906	54
BOPP/PS/PCL-15%-4 × 4	145	0.517 ± 0.003	0.1785	29
BOPP control-5 × 5	–	0.653 ± 0.018	–	–
BOPP/PS-5 × 5	–	0.753 ± 0.018	–	–
BOPP/PS/PCL-5%-5 × 5	27	0.654 ± 0.023	0.1870	–
BOPP/PS/PCL-10%-5 × 5	58	0.375 ± 0.001	0.0680	62
BOPP/PS/PCL-15%-5 × 5	94	0.337 ± 0.010	0.0816	45
BOPP/PS-6 × 6	–	0.818 ± 0.001	–	–
BOPP/PS/PCL-5%-6 × 6	24	0.820 ± 0.111	0.8599	–
BOPP/PS/PCL-10%-6 × 6	45	0.519 ± 0.026	0.1210	–
BOPP/PS/PCL-15%-6 × 6	67	0.470 ± 0.036	0.1378	–

$$P_{\mathrm{eff,PCL}} = \frac{V_{\mathrm{PCL}}}{\frac{1}{P_{\mathrm{film}}} - \frac{V_{\mathrm{BOPP/PS}}}{P_{\mathrm{BOPP/PS}}}} \tag{2}$$

where V_{PCL} and $V_{BOPP/PS}$ are the volume fraction of PCL and PP/PS, and $P_{BOPP/PS}$ is the oxygen permeability of the BOPP/PS control film stretched under the same conditions. The effective permeability of PCL in nanolayers was much lower than in a PCL control. The general trend should be a decrease in $P_{eff,PCL}$ as the layers become thinner [2]. This is due to improved orientation of the in-plane lamellae as the confinement becomes more severe. However, two factors were thought to compromise $P_{eff,PCL}$. The first applied to very thin PCL layers, e.g. thinner than the lamellar thickness, in which case crystallization of PCL with the normal lamellar thickness caused holes to form in the PCL layer. This was thought to be the case with the films having 5% PCL and draw ratios of 5 × 5 and 6 × 6. The second was specific to the nano-BOPP/PS/PCL and occurred when the drawn PS layers were too thin and broke up, thereby exposing the PCL to PP and permitting on-edge crystallization of PCL lamellae. This was thought to be the case with films drawn to 6 × 6. Nevertheless, the effective permeability of PCL in 6 × 6 films was still much lower than in the PCL control. The other data are plotted against PCL layer thickness in Fig. 8. As expected, the $P_{eff,PCL}$ decreased with decreasing the layer thickness. For example, the 45 nm PCL layers of nano-BOPP/PS/PCL-5%-4 × 4 had effective permeability (0.0547 barrer) almost a factor of 20 lower than the permeability of the PCL control (0.983 barrer).

The aspect ratio of the PCL lamellae α was estimated based on the Cussler model [18], assuming that the PCL lamellae were impermeable and oriented perpendicular to the gas flow

$$\frac{P_{\mathrm{film}}}{P_{\mathrm{BOPP/PS}}} = \frac{1-\phi}{1-\phi+(\alpha\phi/2)^2} \tag{3}$$

where ϕ, the volume fraction of PCL lamellae in the film, is obtained from the crystalline phase density (ρ_c = 1.17 g cm^{-3}) and the amorphous phase density (ρ_a = 1.09 g cm^{-3}) of PCL [19], the crystallinity X_c of PCL from DSC (33% by weight), and the volume fraction of PCL in the composite film V_{PCL} as

$$\phi = \frac{\frac{X_c}{\rho_c}}{\left(\frac{X_c}{\rho_c}+\frac{1-X_c}{\rho_a}\right)} \times V_{\mathrm{PCL}} \tag{4}$$

The calculated aspect ratio increases dramatically from about 30 to 100 for the 4 × 4 films as the layers become thinner, Table 2.

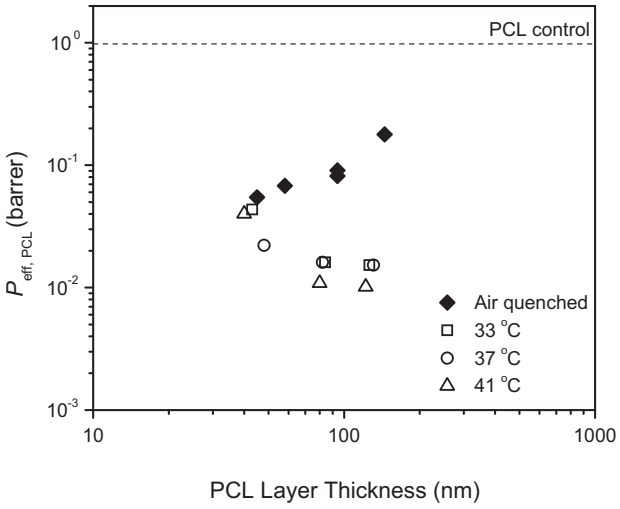

Fig. 8. Effect of isothermal crystallization on the effective oxygen permeability of PCL (draw ratio 4 × 4).

3.3. Isothermal crystallization of PCL in nano-BOPP/PS/PCL

The Brückner has a second oven that was used to isothermally crystallize the PCL layers after the films were stretched. It was anticipated that decreasing the crystallization rate would result in larger PCL lamellae and higher aspect ratios. The nano-BOPP/PS/PCL films were stretched to 4 × 4 and isothermally crystallized at 33 °C (30 min), 37 °C (35 min) and 41 °C (45 min). The crystallization temperatures were in the onset region of the DSC crystallization exotherm (Fig. 7). Because the crystallization temperatures were much lower than the crystallization temperature of PP and the glass transition temperature of PS, the PCL crystallized within solid confinement. Permeability of the isothermally crystallized films and the effective permeability of the PCL nanolayers are given in Table 3. The additional thermal treatment did not affect the permeability of BOPP/PS films within the experimental error. However, isothermal crystallization dramatically affected permeability of the nano-BOPP/PS/PCL films. The isothermally crystallized film had permeability as much as 5× lower than the film that was air-quenched. The remarkable decrease in permeability was attributed to the large aspect ratio of the slowly crystallized PCL lamellae, Table 3. Increasing the crystallization temperature tended to produce films of lower permeability, which was due to the larger lamellae that were obtained with slower crystallization.

The effective permeability of PCL, calculated according to Equation (2), is included in Fig. 8. Isothermal crystallization decreased the permeability of PCL by a factor of 10 compared to the air-quenched films and by almost two orders of magnitude compared to the PCL control (0.983 barrer). Such low oxygen permeability was a result of near perfect in-plane orientation and extremely high aspect ratio of the PCL lamellae.

The effect of humidity on the oxygen permeability was evaluated at 85% RH. The results for the nano-BOPP/PS/PCL films and PCL layers are listed in Table 3. The nano-BOPP/PS/PCL films retained high barrier. In fact, the permeability at 85% RH was slightly lower than at 0% RH. This phenomenon was previously observed in other polymers such as nylon (0–50% RH) [20], and poly(ethylene terephthalate) (0–100% RH) [21]. The decreased permeability was attributed to the filling of free-volume holes with water molecules.

The CO_2/O_2 selectivity, a very important parameter for materials used in food packaging [22,23], was obtained by calculating the ratio of P(CO_2)/P(O_2) directly. Table 3 includes the CO_2/O_2

Table 3
Permeability of isothermally crystallized nano-BOPP/PS/PCL films (draw ratio 4 × 4).

Sample	Nominal PCL layer thickness (nm)	$P(O_2)$ of film P (barrer)	Effective $P(O_2)$ of PCL layer $P_{eff,PCL}$ (barrer)	Aspect ratio of lamellae α	$P(O_2)$ of film at 85%RH P_{85} (barrer)	Effective $P(O_2)$ of PCL layer at 85% RH $P_{eff,PCL,85}$	$P(CO_2)/P(O_2)$ of film (barrer)
BOPP/PS-air-quenched	–	0.777 ± 0.002	–	–	–	–	–
BOPP/PS-33 °C	–	0.794 ± 0.010	–	–	0.696 ± 0.015	–	4.5
BOPP/PS-37 °C	–	0.822 ± 0.036	–	–	0.707 ± 0.012	–	4.5
BOPP/PS-41 °C	–	0.810 ± 0.017	–	–	0.677 ± 0.004	–	4.6
BOPP/PS/PCL-5%-air-quenched	45	0.468 ± 0.003	0.0547	–	–	–	–
BOPP/PS/PCL-5%-33 °C	43	0.426 ± 0.010	0.0424	–	0.368 ± 0.022	0.0370	5.7
BOPP/PS/PCL-5%-37 °C	48	0.293 ± 0.004	0.0222	–	0.225 ± 0.001	0.0161	6.7
BOPP/PS/PCL-5%-41 °C	40	0.413 ± 0.013	0.0400	–	0.347 ± 0.020	0.0338	6.1
BOPP/PS/PCL-10%-air-quenched	94	0.442 ± 0.033	0.0904	54			
BOPP/PS/PCL-10%-33 °C	84	0.136 ± 0.002	0.0161	135	0.103 ± 0.007	0.0119	9.0
BOPP/PS/PCL-10%-37 °C	82	0.137 ± 0.002	0.0161	138	0.104 ± 0.007	0.0120	8.2
BOPP/PS/PCL-10%-41 °C	80	0.097 ± 0.002	0.0109	167	0.074 ± 0.003	0.0082	9.0
BOPP/PS/PCL-15%-air-quenched	145	0.517 ± 0.003	0.1785	29	–	–	–
BOPP/PS/PCL-15%-33 °C	126	0.092 ± 0.003	0.0153	112	0.062 ± 0.019	0.0101	9.0
BOPP/PS/PCL-15%-37 °C	131	0.092 ± 0.002	0.0153	115	0.046 ± 0.001	0.0073	8.8
BOPP/PS/PCL-15%-41 °C	122	0.063 ± 0.002	0.0101	140	0.044 ± 0.005	0.0070	9.0

selectivity of the nano-BOPP/PS/PCL films. Selectivity was 16.0 for the PCL control, 4.8 for the PS control and 4.5 for the BOPP control. As expected, the PCL layers increased the selectivity of the nano-BOPP/PS/PCL films as high as 9.0. The increase in selectivity was more significant than the additive calculation based on composition. High selectivity was achieved with very low PCL content. The series model indicated that the permeation properties including selectivity of the layered structure were dominated by the component with the lowest permeability.

3.4. Clarity and toughness of nano-BOPP/PS/PCL

In addition to gas barrier, clarity and toughness are key properties of BOPP film. The isothermally crystallized nano-BOPP/PS/PCL films retained excellent see-through clarity. No difference could be discerned between the BOPP control and nano-BOPP/PS/PCL films by eye. The BOPP control film had light transmission of about 90%, Fig. 9. Incorporating PCL and PS nanolayers in the BOPP did not have much effect of the light transmission which remained at 85–90%, although a slight decrease was observed with increasing PCL content. In order to remove the contribution of surface roughness to the light scattering, a refractive index matching oil was spread on both sides of the film. The results are

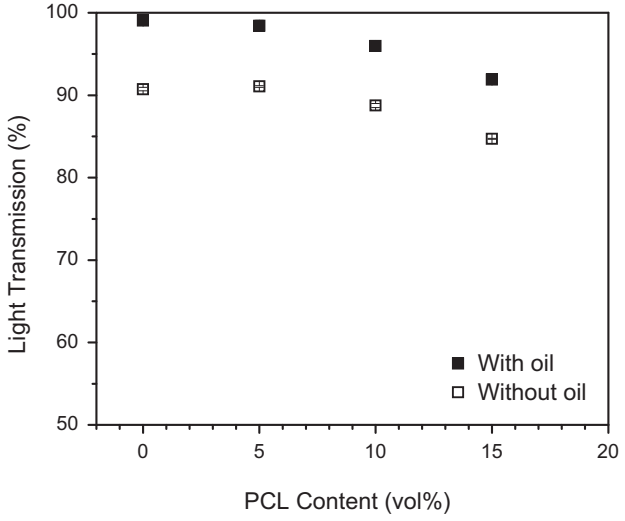

Fig. 9. Light transmission of nano-BOPP/PS/PCL films (draw ratio 4 × 4).

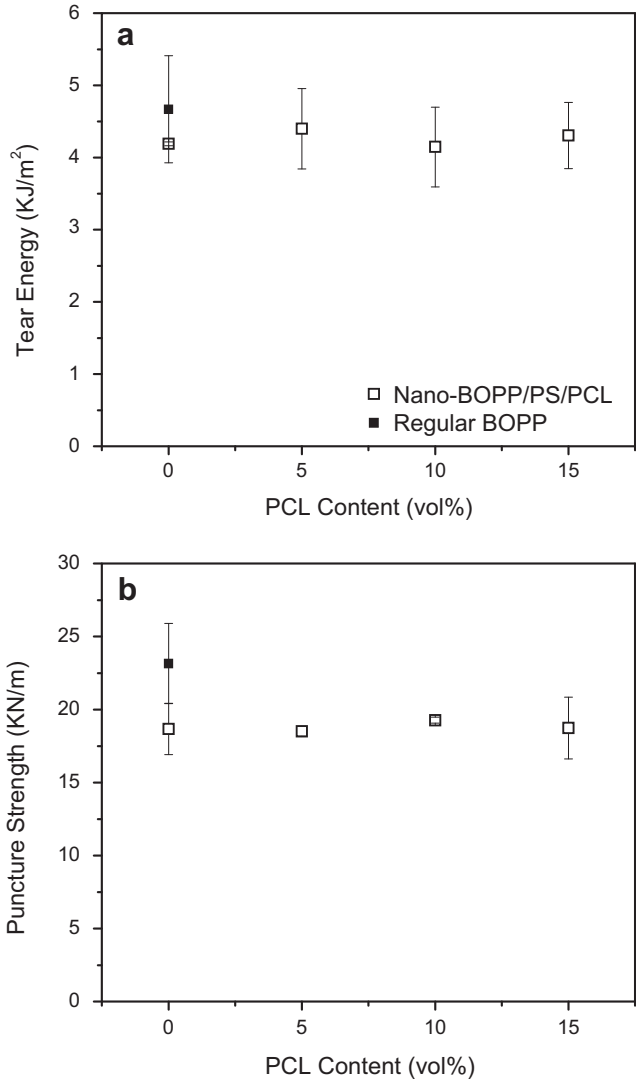

Fig. 10. Mechanical properties of nano-BOPP/PS/PCL films: (a) tear energy, and (b) puncture strength (draw ratio 4 × 4).

included in Fig. 9. For the BOPP control film, the light transmission increased almost to 100%. Similarly, the light transmission for nano-BOPP/PS/PCL films also increased close to 100%. Again, a slight decrease in the light transmission was observed for the nano-BOPP/PS/PCL films with higher PCL content, although the difference was difficult to detect by eye. The effect was attributed to the increase in PCL layer thickness. When the PCL content was low, the PCL layer thickness fell comfortably below the quarter wavelength of visible light. At this layer thickness, light would not scatter from the layer interfaces even though the refractive indices did not match. As the PCL content increased, the layer thickness approached the quarter wavelength and the layers might have been thick enough that some small amount of light was scattered.

Mechanical properties including tear resistance and puncture strength were also tested. The biaxial orientation resulted in balanced mechanical properties in the two stretching directions. Fig. 10a shows the tear energy of the isothermally crystallized nano-BOPP/PS/PCL and BOPP/PS films. The tear energy G_t is calculated as

$$G_t = \frac{2F_t}{t} \tag{5}$$

where F_t is the steady force during the tear test and t is the thickness of the film. Incorporation of PCL layers did not affect the tear energy of the films. Fig. 10b shows the puncture strength of the annealed nano-BOPP/PS/PCL and BOPP/PS films. The puncture strength G_p is calculated as

$$G_p = \frac{F_p}{t} \tag{6}$$

where F_p is the highest force when the needle penetrates through the film. The PS layers of nano-BOPP/PS reduced the performance in both tear and puncture slightly, however this slight decrease can be neglected from application point of view. Addition of PCL layers of nano-BOPP/PS/PCL did not produce any additional change. Mechanical properties of BOPP films were well retained.

4. Conclusions

The gas permeability of BOPP films can be improved only by a factor of about 2 through the biaxial orientation process. Further improvement is possible by reinforcement or coextrusion with a higher barrier constituent, however the modification must have nanoscale dimensions if good clarity is to be conserved. Using a layer-multiplying, forced assembly process to incorporate the high barrier constituent, we achieved an order of magnitude improvement in the oxygen barrier of BOPP films. The improvement was obtained without sacrificing film clarity and toughness. The novel approach exploited a recent finding that under 2D confinement in nanolayers, PEO crystallizes as large, in-plane lamellae that resemble single crystals. This crystallization habit imparts more than 2 orders of magnitude reduction in oxygen permeability. Because the permeability of PEO is compromised under humid conditions, we sought another polymer that would also crystallize under confinement as large, in-plane lamellae. A candidate polymer was PCL. However, the lamellae in PCL nanolayers were found to be oriented perpendicular to the film surface, which actually facilitated oxygen permeation through the PCL layers and increased the oxygen permeability of the oriented films. Crystallization as on-edge lamellae was attributed to nucleation by the polypropylene surface. The surface nucleation was prevented by inserting buffer PS layers in between the PCL and PP layers. In this case, the PCL lamellae were oriented in-plane. With the high aspect ratio lamellar crystals oriented perpendicular to the flux direction, the increased tortuosity of the diffusion pathway improved the oxygen barrier significantly. The aspect ratio of the PCL lamellae was maximized by isothermal crystallization, which further increased the tortuosity of the permeation pathway and produced the largest improvements in oxygen barrier. Because the permeation properties including selectivity were dominated by the least permeable constituent, the CO_2/O_2 selectivity of the films with PCL nanolayers increased dramatically as compared to the control BOPP films. This demonstrates how polymer nanolayers can be incorporated into the design of conventional polymeric films in order to obtain the right barrier properties.

Acknowledgments

This research was supported by the NSF Center of Layered Polymeric Systems (Grant DMR-0423914).

References

[1] Wang HP, Keum JK, Hiltner A, Baer E, Freeman B, Rozanski A, et al. Science 2009;323:757–60.
[2] Wang HP, Keum JK, Hiltner A, Baer E. Macromolecules 2009;42:7055–66.
[3] Lüpke T, Dunger S, Sanze J, Radusch HJ. Polymer 2004;45:6861–72.
[4] Lin YJ, Dias P, Chen HY, Hiltner A, Baer E. Polymer 2008;49:2578–86.
[5] Gupta M, Lin YJ, Deans T, Crosby A, Baer E, Hiltner A, et al. Polymer 2009;50:598–604.
[6] Hu YS, Prattipati V, Mehta S, Schiraldi DA, Hiltner A, Baer E. Polymer 2005;46:2685–98.
[7] Kamal MR, Garmabi H, Hozhabr S, Arghyris L. Polym Eng Sci 1995;35:41–51.
[8] Yeh JT, Yao WH, Du QG, Chen CC. J Polym Sci Part B Polym Phys 2005;43:511–21.
[9] Usuki A, Kojima Y, Kawasumi M, Okada A, Fukushima Y, Kurauchi T, et al. J Mater Res 1993;8:1179–84.
[10] Kojima Y, Usuki A, Kawasumi M, Okada A, Fukushima Y, Kurauchi T, et al. J Mater Res 1993;8:1185–9.
[11] Paul DR, Robeson LM. Polymer 2008;49:3187–204.
[12] Lin YJ, Hiltner A, Baer E. Polymer 2010;51:4218–24.
[13] Lin YJ, Dias P, Chum S, Hiltner A, Baer E. Polym Eng Sci 2007;47:1658–65.
[14] Dias P, Lin YJ, Hiltner A, Baer E, Chen HY, Chum SP. J Appl Polym Sci 2008;107:1730–6.
[15] Liu JC, Li HH, Yan SK, Xiao Q, Petermann J. Colloid Polym Sci 2003;281:601–7.
[16] Yan C, Li HH, Zhang JM, Ozaki Y, Shan DY, Yan DD, et al. Macromolecules 2006;39:8041–8.
[17] Balsamo V, Gouveia LM. J Polym Sci Part B Polym Phys 2007;45:1365–79.
[18] Cussler EL, Hughes SE, Ward WJ, Aris R. J Memb Sci 1998;38:161–74.
[19] Lefevre C, Villers D, Koch MHJ, David C. Polymer 2001;42:8769–77.
[20] Hu YS, Mehta S, Schiraldi DA, Hiltner A, Baer E. J Polym Sci Part B Polym Phys 2005;43:1365–81.
[21] Auras R, Harte B, Selke S. J Appl Polym Sci 2004;92:1790–803.
[22] Kader AA, Zagory D, Kerbel EL. Crit Rev Food Sci 1989;28:1–30.
[23] Lee LL, Arul J, Lencki R, Castaigne F. Packag Technol Sci 1996;9:55–72.